Graphene allotropes under extreme uniaxial strain: An ab-initio theoretical study.

Zacharias G. Fthenakis[1,2] and Nektarios N. Lathiotakis[3,4]

[1] *Physics and Astronomy Department, Michigan State University, East Lansing, Michigan 48824, USA*
[2] *Institute of Electronic Structure and Laser, FORTH, P.O. Box 1527, 71110 Heraklio, Crete, Greece*
[3] *Theoretical and Physical Chemistry Institute, National Hellenic Research Foundation, Vass. Constantinou 48, GR-11635 Athens, Greece*
[4] *Max-Planck-Institut für Mikrostrukturphysik, Weinberg 2, D-06120 Halle (Saale), Germany*

(Dated: March 31, 2015)

Pentaheptites and Octagraphene are allotropes of graphene that have been predicted theoretically although less favorable energetically than graphene. In this work, we use density functional theory calculations, to study the response of two representative Pentaheptites and Octagraphene upon uniaxial strain up to the fracture limit. We calculate their mechanical properties like Young's modulus, Poison's ratio and speed of sound. We also determine their ultimate tensile strength and the corresponding strain, and describe the pathways of their fracture. Finally, we focus on their relative stability compared to graphene under strain. We find that under uniaxial strain of the order of 10-12% in certain directions, which we determine, pentaheptites become energetically favorable than graphene. The energy barriers for the transitions decrease dramatically under strain, however, they remain prohibitive for structural transitions. Thus, strain alone can not provide a synthetic route to these allotropes, but could be a part of composite procedures for this purpose.

PACS numbers:

I. INTRODUCTION

The rise of graphene era, which followed its isolation and identification[1], has inevitably fueled the interest on alternative two dimensional materials, like boron nitride[2,3], metallic dichalcogenides[4], graphene allotropes[5] (i.e. entirely planar three-fold coordinated Carbon structures), etc. Theoretically, several graphene allotropes has been predicted to be stable[6–10]. A class of them, known as "haeckelites"[6,8–10], can be derived from graphene upon extensive periodically arranged Stone-Wales transformations (SWTs)[11,1258].

Theoretical investigations on haeckelites started at middle '90s by Crespi et al[6], who proposed and studied the electronic properties of a pentaheptite structure (i.e. a haeckelite built entirely out of pentagonal and heptagonal carbon rings), finding that it is planar, metallic and at least as stable as C_{60}. A few years later, Terrones et al[10], who introduced the term "haeckelites", studied the stability and electronic, mechanical and vibrational properties of three such structures and their nanotube counterparts[10,13]. Another haeckelite, which has received attention recently[5,14–19] is the so-called octagraphene[14] (OcGr) or T-graphene[15], which is built entirely of square and octagonal carbon rings. Apparently, there is a whole world of complex planar-sp^2 carbon allotropes consisting partially of hexagons and/or pairs of heptagons-pentagons and/or squares-octagons. In the last decade, the properties of these (see for instance Refs. 20–22), as well as several other similar periodic[9,23–26], and amorphous[27] haeckelite structures, has been investigated. Haeckelites could have unique and maybe tailored properties of technological interest. For instance, they can be either metallic or not[23], or they can be planar or buckled, depending on the arrangement of the SWTs[59].

Despite the theoretical predictions for their stability, periodic haeckelite structures have not been synthesized yet. On the other hand, structures based on SWTs or similar transformations have been observed and/or synthesized experimentally. Such structures include graphene with point SW defects[28], amorphous haeckelite structures[27,29], haeckelite-like 5-7 or 5-8 line defects[30,31], grain boundaries[32], grain boundary loops of pentagons and heptagons[33] and reconstructed graphene edges of alternating pentagonal and heptagonal carbon rings[34]. This fact indicates that periodic haeckelite structures could be synthesized in the future. It is also worth to mention the reknitting process[35], which spontaneously takes place in graphene nanoholes, by filling up with non hexagonal carbon rings.

Among the possible haeckelite synthetic routes[6,26], the direct one, by rotating appropriate C-C bonds of the graphene lattice, seems to be prohibitive, since there is a huge energy barrier for this process. According to Crespi et al[6], this barrier is of the order of 7 eV attributed to the breaking of two C-C bonds along the rotation pathway. An even higher value of 9.2 eV has also been reported[36]. On the other hand, this barrier has been shown theoretically to reduce substantially through catalytic paths in the presence of external atoms[37], using Boron doping[38], or upon strain, as reported by Samsonidze et al[39] using an atomistic model.

Although most of the theoretical studies on haeckelites focus on their stability and electronic properties, little has been done on their response to stress[7,14,40,41]. In the present work, we attempt to cover this gap. Experimentally, large uniaxial stress, up to the fracture limit, has been applied to a graphene monolayer[42], measuring its ultimate tensile strength (UTS) and the correspond-

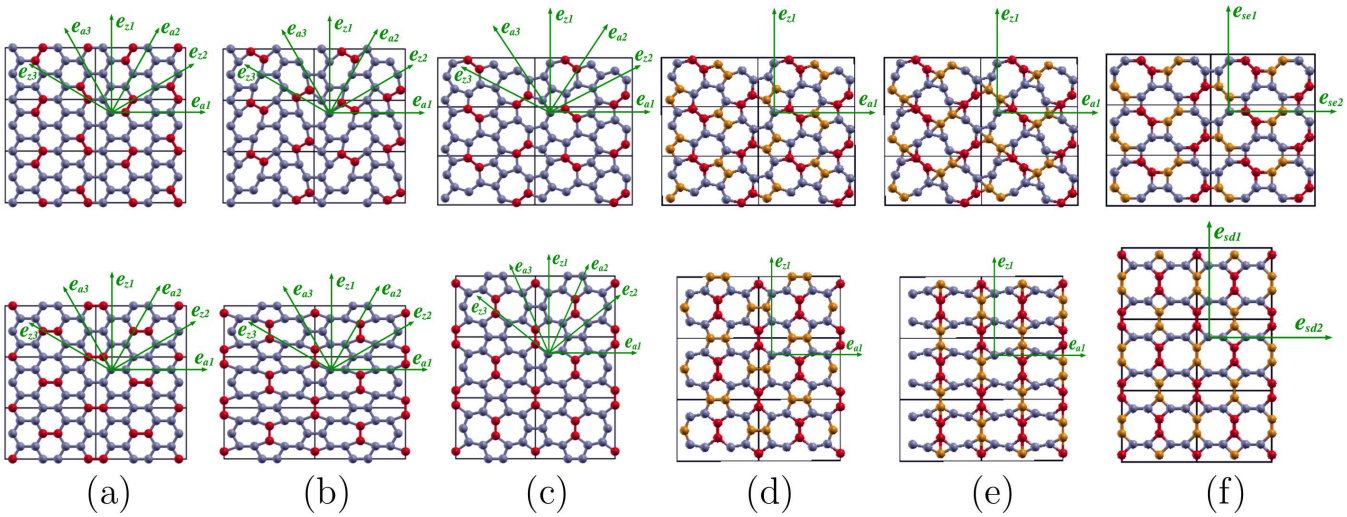

FIG. 1: Conversion of graphene into PeHe-A ((a)-(c) top) and PeHe-B ((a)-(c) bottom) and their further conversion to OcGr (d)-(f) through a periodic mesh of SWTs. The green arrows show the strain directions considered in our study: (a) Graphene and the mesh of rotating bonds in red; (b) 90° rotations have been performed in the otherwise unperturbed graphene lattice; (c) PeHe-A (top) and PeHe-B (bottom) structures upon energy optimization; (d) PeHe-A and PeHe-B structures, with the additional rotating bonds (in orange) leading in both cases to OcGr; (e) 90° rotations have been performed in the otherwise unperturbed PeHe-A and PeHe-B lattices; (f) the final optimized OcGr structures.

ing strain $\varepsilon = 0.25$. Of course, a relevant question is whether graphene remains energetically more stable than its planar allotropes in the regime of so large uniaxial deformation. In the present, we also attempt to answer this question.

More specifically, we consider two periodic pentaheptite structures, which we call PeHe-A and PeHe-B (see Fig. 1(c), top and bottom panels, respectively) and OcGr (Fig. 1(f) top and bottom) and we study their mechanical properties for uniaxial stretching in comparison with graphene, up to the fracture limits, using *ab-initio* density functional theory (DFT) calculations. We plot their stress-strain curves and calculate their Young's modulus, Poisson's ratio, speed of sound, and ultimate stress - strain limits for different strain directions. Additionally, we examine if strain can be an assisting factor for their synthesis. For this purpose, we determine the strain directions that might favor their relative stability (compared with graphene) and check for the existence of crossing points in the curves of the total energies as a function of strain along these directions. Finally, using a prototype molecular system, we estimate the energy barrier for SWTs as a function of strain.

The present paper is organized as follows: In Sect. II, we describe the structures we considered and the periodic SWTs that lead to them, as well as our methodology. In Sect. III, we present and discuss our results on the equilibrium and mechanical properties of the allotropes (Sect. III A), their UTS and fracture patterns (Sect. III B), and finally their relative stability as a function of uniaxial strain (Sect. III C). The conclusions are included in Sect. IV.

II. STRUCTURES AND METHOD

In Fig. 1(a)-(c), we show the mechanism of conversion of graphene into PeHe-A and PeHe-B (top and bottom panels, respectively) through periodic arrangements of SWTs. The bonds in graphene (a) colored in red have been rotated by 90° in (b) and the relaxed PeHe-A and PeHe-B structures are shown in (c). We note that PeHe-B is the pentaheptite structure introduced by Crespi et al[6]. Furthermore, in Fig. 1(d)-(f), we show the conversion mechanism of PeHe-A and PeHe-B (top and bottom panels, respectively) to OcGr. The rotation by 90° of all the common bonds of adjacent pentagons (colored in orange) in either PeHe-A ((d)(top)) or PeHe-B ((d)(bottom)), lead to the structures in (e) which upon optimization relax to OcGr in (f). The structures in the top and bottom panels in (f) are identical but rotated with respect to each other by 45°.

Due to the symmetry reduction associated with the arrangement of SWTs, the primitive unit cells in PeHe-A, PeHe-B and OcGr contain 16, 8 and 4 atoms, respectively. For the purposes of the present study, we adopt a common rectangular 16-atom unit cell, shown with black lines in Fig. 1.

In order to investigate the response of the structures under study to strain, we optimize them under constant strain along certain representative high symmetry directions. For graphene, PeHe-A and PeHe-B these directions are defined in terms of fractional coordinates, with respect to the selected rectangular unit cell vectors: (0,1), (1,1), (-1,1), (1,0), (1,3) and (-1,3). They are shown in Fig. 1(a-c) denoted as e_{z1}, e_{z2}, e_{z3}, e_{a1}, e_{a2}, e_{a3}, respectively. For graphene, they correspond to the three

equivalent directions along zig-zag (e_{z1}, e_{z2}, e_{z3}) and the three equivalent directions along arm-chair chains (e_{a1}, e_{a2}, e_{a3}) which we will simply call zig-zag and arm-chair directions. Occasionally we will use the notation e_a, e_z referring to them. However, for PeHe-A and PeHe-B, only e_{z1}, e_{z2}, e_{a1} and e_{a2} are different from each other, since under the structural transformations $x \to -x + c_x$ and $y \to y + c_y$, (for certain constant values of c_x and c_y) for PeHe-A, and $x \to -x$ for PeHe-B, e_{z3} and e_{a3} coincide with e_{z2} and e_{a2}, respectively. In the present study, we focus on the effect of strain in the directions e_{a1}, e_{z1} and e_{z2} for PeHe-A and e_{a1}, e_{z1}, e_{a2} for PeHe-B. In the case of e_{z2} and e_{a2}, a non-rectangular unit cell is adopted, as required in order to keep the same number of atoms per unit cell. After the conversion of PeHe-A and PeHe-B to OcGr, shown in Fig. 1 (d)-(f), the directions e_{a1} and e_{z1} become equivalent in both cases. Thus, to avoid confusion, for OcGr, we adopt the notation e_{se} (direction along a square edge), and e_{sd} (along square diameter). In the case of PeHe-A conversion, e_{a1} and e_{z1} become e_{se1}, e_{se2}, while for PeHe-B they become e_{sd1}, e_{sd2}, respectively.

For our calculations, we used the Quantum Espresso[43] periodic DFT code at the level of GGA/PBE functional[44]. We adopted an ultra-soft pseudopotential[45] for C, generated by a modified RRKJ approach[46]. We used k-meshes of the order of 6×12 points which were found sufficient to converge structural properties given the relatively large size of the adopted unit-cell. We chose cutoffs 50 and 500 Ryd for the wave functions and charge density, respectively and occupation smearing of 5 mRyd. Calculations under constant strain were performed by scaling and freezing the corresponding unit-cell vector while all the rest of the structural parameters, i.e. atom positions and cell dimensions, were fully optimized.

III. RESULTS AND DISCUSSION

A. Structural and mechanical properties

According to our findings, the optimized PeHe-A and PeHe-B structures are by 0.22 and 0.24 eV per atom, respectively, less favorable than graphene. The optimized OcGr structure is by 0.25 eV per atom higher than PeHe-B. Based on those energy differences and bearing in mind, that two SWTs take place per unit cell for the formation of PeHe-A and PeHe-B, and two more for the formation of OcGr, the energy cost for a SWT is $\approx 1.8 - 2.0$ eV.

As seen in Fig. 1(c), the lattice of PeHe-A and PeHe-B remains rectangular upon optimization. However, the lattice parameter of PeHe-A in the e_{a1} direction increases while that of the e_{z1} decreases. In the case of PeHe-B, we have the opposite, i.e. the lattice parameter increases along the e_{z1} direction and decreases along the e_{a1}. For PeHe-B, this change in dimensions looks plausible since the structure is enlarged in the direction that the bonds turn to, as a stress reduction mechanism. For PeHe-A, a similar mechanism takes place although the bonds are never parallel to any of the lattice vectors. Similarly, however, enlargement of the structure occurs in the direction with the largest projection of the rotated bonds. The magnitude of the lattice vectors for the rectangular lattice of PeHe-A and PeHe-B, shown in Fig. 1, are $a_x = 9.157$ Å and $a_y = 4.749$ Å for PeHe-A, and $a_x = 7.460$ Å and $a_y = 5.847$ Å for PeHe-B, respectively. The magnitude of the corresponding lattice vectors for graphene is $a_{g,x} = 6a_0 = 8.531$ Å and $a_{g,y} = 2\sqrt{3}a_0 = 4.925$ Å, where $a_0 = 1.422$ Å is the bond length. For the square lattice of OcGr, the lattice constant a is $a = 2(a_1 + \sqrt{2}a_2) = 6.877$ Å, where $a_1 = 1.370$ Å and $a_2 = 1.462$ Å are the bond lengths corresponding to the adjacent octagon edges and the square edges, respectively.

We calculate the response of PeHe-A, PeHe-B and OcGr as well as graphene for uniaxial stress σ, for strains ε ranging from -20% up to 30%. As it is customary, to obtain values relevant for comparison with 3-dimensional materials[42,47] we consider a structure thickness of 3.34 Å (the interlayer separation distance of graphite).

Obviously, any 2-dimensional (2D) structure under compression would prefer to bend instead of remaining flat and negatively strained[50]. However, it is possible to perform calculations for negative strains, without structure bending, in order to estimate, more reliably, quantities that are expressed as derivatives $dA/d\varepsilon$, or as ratios A/ε, at $\varepsilon = 0$, using least square fitting, rather than extrapolating positive strain results to $\varepsilon = 0$. Such quantities are the Young's modulus E, ($E = \sigma/\varepsilon$), and the Poisson's ratio ν, ($\nu = -\varepsilon_\perp/\varepsilon$, where $\varepsilon_\perp$ is the transverse strain).

In Fig. 2(a), we show the stress-strain curves for all structures in the range $0 \leq \varepsilon \leq 0.3$. In agreement with other theoretical[47–49,51,52] and experimental[42] studies in graphene, we find a non linear stress-strain relation not only for graphene, but also for the allotropes of our study, even for stress less than 5%. For graphene, it has been proposed[42] that this non-linear behavior can be expressed as $\sigma = E\varepsilon + D\varepsilon^2$ (which is equivalent to a linear dependence of σ/ε on ε), although an even higher order expansion in strain has been considered[48]. However, as shown in Fig. S1(c) of the Supplemental Information, the dependence of σ/ε on ε diverges from linearity for the strain range we considered and for all structures. We found more accurate description a fitting to the quadratic equation

$$\sigma/\varepsilon = E + D\varepsilon + F\varepsilon^2, \tag{1}$$

for $0 < \varepsilon \lessapprox \varepsilon_u$, where ε_u is the strain corresponding to the UTS. The fitting lines are presented in Fig. 2(a) and Fig. S1(c) of the Supplemental Information. However, D and F depend strongly on the range of ε, or the fitting method, indicating that even a fitting using Eq. (1) can not provide reliable values for D and F (see Supplemental Information for more details).

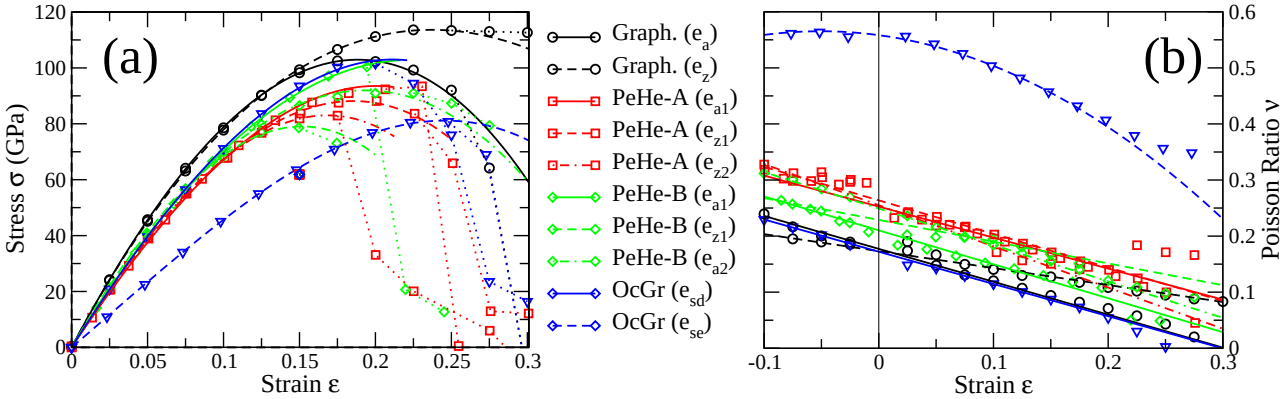

FIG. 2: (a) Stress - strain curve and (b) Poison's ratios as a function of strain, for Graphene, PeHe-A, PeHe-B, and OcGr for different strain directions. The straight, dashed and dot-dashed lines in the stress - strain graph are the fitting lines according to Eq. (1), (2) for (a) and (b), respectively. The dotted lines in (a) connect the stress - strain points for strain values $\varepsilon \gtrapprox \varepsilon_u$.

Structure	Source/Method	Direction	E (GPa)	ν	ρ (gr/cm^3)	v_s (km/sec)	ε_u	σ_u (GPa)
Graphene	present work	e_a	**1024**	**0.177**	**2.291**	**21.14**	**0.185**	**103**
	present work	e_z	**1020**	**0.173**	**2.291**	**21.10**	**0.225**	**114**
	LDA [41]	e_a, e_z	1054	0.185	(2.314)	(21.34)		
	LDA [47]	e_a, e_z	1050	0.186	(2.313)	(21.30)	0.194	110, 121
	GGA/PBE [48]	e_a, e_z	1042	0.169	(2.323)	(21.18)		118
	GGA/PBE [41]	e_a, e_z	1025	0.173	(2.277)	(21.22)		
	GGA/PW [14]	e_a, e_z	1048	0.17	(2.305)	(21.32)		104, 115
	Atomistic[49]	e_a, e_z	960	0.22	(2.29)	(20.47)		100, 120-130
	Exp. [42]		1020 ± 150				0.25	126 ± 12
PeHe-A	present work	e_{a1}	**825**	**0.253**	**2.213**	**19.3**	**0.240**	**94**
	present work	e_{z1}	**860**	**0.264**	**2.213**	**19.7**	**0.192**	**88**
	present work	e_{z2}	**865**	**0.255**	**2.213**	**19.8**	**0.169**	**83**
PeHe-B	present work	e_{a1}	**882**	**0.210**	**2.207**	**20.0**	**0.201**	**101**
	present work	e_{z1}	**937**	**0.229**	**2.207**	**20.6**	**0.144**	**79**
	present work	e_{a2}	**897**	**0.249**	**2.207**	**20.2**	**0.214**	**91**
	GGA/PBE [41]	e_{a1}	885	0.208	(2.196)	(20.1)		
	GGA/PBE [41]	e_{z1}	929	0.218	(2.196)	(20.6)		
OcGr	present work	e_{sd}	**866**	**0.172**	**2.035**	**20.6**	**0.193**	**102**
	present work	e_{se}	**461**	**0.558**	**2.035**	**15.1**	**0.238**	**82**
	GGA/PBE [41]	e_{sd}	854	0.185	(2.021)	(20.6)		
	GGA/PW [14]	e_{sd}	916	0.13	2.036	(21.2)		103
	GGA/PW [14]	e_{se}	503	0.47	2.036	(15.7)		82

TABLE I: Calculated Young's modulus E, Poisson's ratio ν, mass density ρ, speed of sound v_s, UTS σ_u and the corresponding strain values ε_u in different directions for graphene, PeHe-A, PeHe-B and OcGr compared with other values reported. Values in parenthesis are not provided in, but evaluated using data from, the corresponding publication.

Young's moduli E have been estimated by fitting a 3rd degree polynomial of the form $\sigma = F\varepsilon^3 + D\varepsilon^2 + E\varepsilon$ to the (ε, σ) values for ε in the range $-0.1 \leq \varepsilon \leq 0.1$ (Supplemental Information, Fig. S1(a)). For Poisson's ratio ν at ambient strain we fitted a quadratic equation of the form

$$\varepsilon_\perp = \nu_1 \varepsilon^2 - \nu\varepsilon \tag{2}$$

to the (ε, $\varepsilon_\perp$) values for the same ε range (Fig. S1(b) of the Supplemental Information). The obtained values of Young's modulus and Poisson's ratio are presented in Table I together with other theoretical and experimental values.

As we see in Fig. 2 and Table I, all structures appear to be quite isotropic in terms of stiffness and Poisson's ratio with OcGr being a striking exception. As expected, graphene exhibits isotropic behavior along e_a and e_z directions, with the highest E value among all structures. The anisotropy for graphene of $\approx 0.2\%$ and $\approx 1\%$ on the average for Young's modulus and Poisson's ratio, respectively, can be attributed to numerical errors. The anisotropy of PeHe-A and PeHe-B is $\approx 5-6\%$ for stiffness, while for the Poisson's ratio it is $\approx 5\%$ and $\approx 20\%$ for PeHe-A and PeHe-B, respectively.

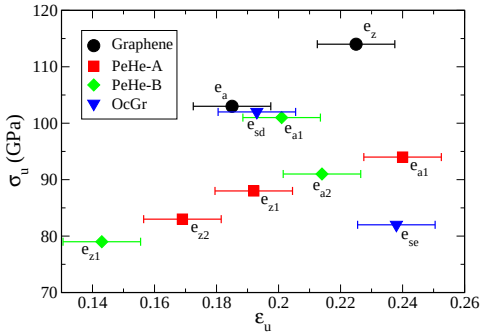

FIG. 3: Ultimate tensile stress σ_u versus ε_u.

The structures under investigation can be sorted in terms of stiffness, from the highest to the lowest E values as: graphene > PeHe-B > OcGr(e_{sd}) $\gtrapprox$ PeHe-A > OcGr(e_{se}). In terms of Poisson's ratio from the lowest to the highest ν they can be sorted as: OcGr(e_{sd}) $\lessapprox$ graphene < PeHe-B < PeHe-A < OcGr(e_{se}). The highly anisotropic behavior of OcGr has been studied and explained in detail elsewhere[53], and it has been attributed to the topology of OcGr.

Using the obtained values for E, we can calculate the longitudinal speed of sound $v_s = \sqrt{E/\rho}$ (ρ is the mass density), for the corresponding direction. The values of v_s for all the structures and the strain directions we considered are presented in Table I. As one can see, graphene exhibits the highest v_s value. Excluding OcGr in the e_{se} direction, all allotropes (including graphene) exhibit high v_s values, ranging between 19.3 and 21.14 km/sec. Similar v_s values have been reported for PeHe-A, PeHe-B and graphene (19.7, 20.0 and 24.0 km/sec, respectively)[22] using the slope at Γ point of the phonon dispersion obtained with the use of the Tersoff interatomic potential.

B. Ultimate tensile strength and fracture

We estimate the UTS, σ_u, corresponding to an ultimate strain ε_u, by fitting a quadratic function for the stress-strain curve in the region of the highest strain values. Our results are presented in Fig. 3, as well as in the Table I, together with results form the literature. The half of strain step $\delta\varepsilon/2 = 0.0125$ adopted in our calculations can be considered as the estimated error for ε_u. For all the structures and strain directions, σ_u is extremely high in comparison with that of common high-UTS materials and are comparable to those of graphene, which exhibit the highest σ_u for both e_z and e_a strain directions.

The behavior of OcGr, PeHe-A and PeHe-B under strain in different directions is shown in Figs. 4-8. The series of snapshots in these figures, show the structural changes for increasing ε. In each successive snapshot, at least one additional bond exceeds in length the 1.65 Å, assuming that breaking starts at this value. Bonds, candidates for breaking, are those with the highest elongation. Naturally, such bonds are those which are either directed along or with a small angle to the strain direction. The best examples are bonds in graphene and OcGr. Indeed, for OcGr, the bonds that break are those corresponding to the adjacent octagon edges (for stress along e_{sd} direction), or the square edges (for strain along e_{se} direction), as shown in Fig. 4. For the e_{sd} and e_{se}

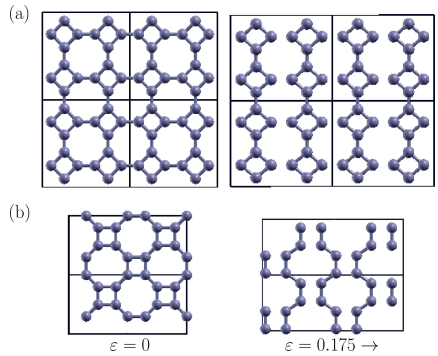

FIG. 4: Snapshots of OcGr for specific strain values along (a) e_{sd} and (b) e_{se} directions. Bonds start breaking in both cases at $\varepsilon = 0.175$. The arrows next to the strain values indicate the strain direction.

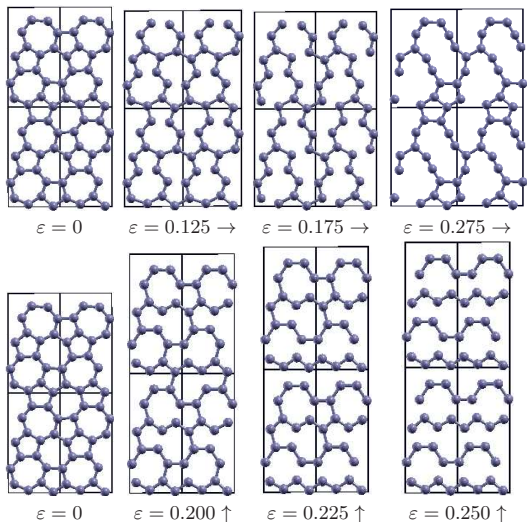

FIG. 5: Snapshots of PeHe-A for specific strains along e_{z1} (top) and e_{a1} (bottom). The arrows show the strain direction.

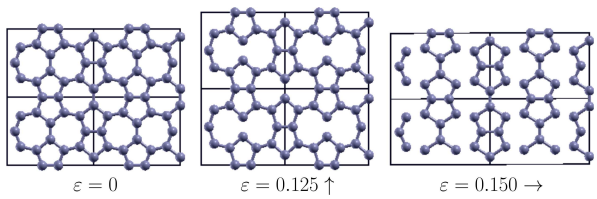

FIG. 6: Snapshots of PeHe-B for specific strains along e_{z1} (center) and e_{a1} (right). The arrows show the strain direction.

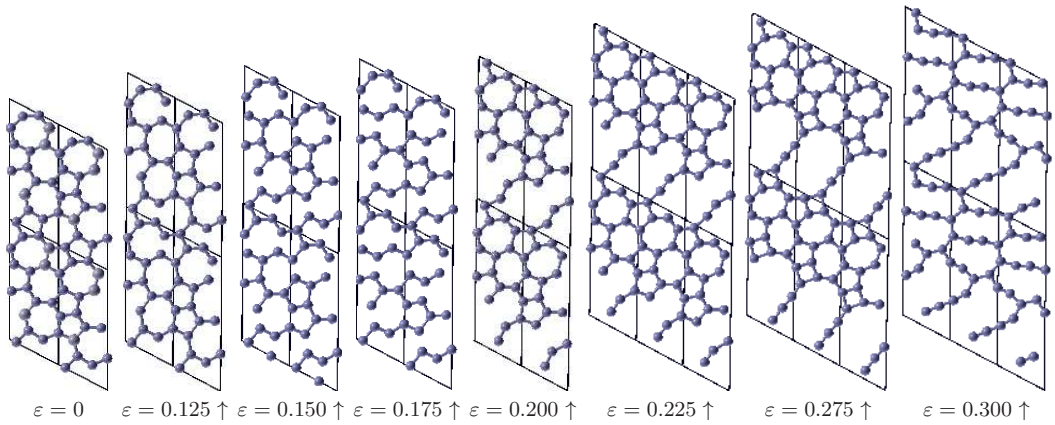

FIG. 7: Snapshots of PeHe-A for specific strain values along e_{z2}. The arrows show the strain direction.

strain directions and for $\varepsilon > \varepsilon_u$, OcGr was found to break into lines of interconnected squares or arm-chair chains. For even higher ε, e.g. $\varepsilon \gtrapprox 0.275$, straight carbene chains are obtained.

For graphene strained along e_a direction, the bonds are either at an angle of $\pm 60^o$ with respect to the strain direction, or they are parallel to the strain direction. It is expected therefore, that the latter will break first, creating, theoretically, zig-zag chains. On the other hand, for graphene strained along e_z direction, the bonds are either at an angle of 30° or vertical to the strain direction. Therefore, bonds in the zig-zag chains will break first, leading, theoretically, to carbon dimers. In reality, however, more complicated structures will be the products of fracture since not all bonds will break simultaneously. In the fracture processes for graphene, described above, one bond per atom breaks for strain along e_z direction, while half a bond per atom breaks for strain along e_a direction. This explains why UTS for the e_z direction is higher than that for the e_a, as seen in Fig. 3 and Table I. The theoretically obtained fracture strain for both directions is higher than the maximum value 0.3, of our study. It is also much higher than the experimental value, due to effects owe to the finite size of the supercell, temperature and defects.

Under extreme strain, i.e. for values higher than ε_u, the investigated allotropes either dissociate into linear chains, or undergo a transition to structures containing carbene units accompanied by bond recreation, like PeHe-A strained along e_{z1} and e_{z2} directions, and PeHe-B strained alone e_{a2} direction. Those chains are either zig-zag or arm-chair chains (graphene e_a, OcGr e_{se}, PeHe-A e_{a1}, PeHe-B e_{a2}), or they are composed of interconnected squares (OcGr e_{sd}), or couple of adjacent pentagons (PeHe-B e_{a1}). For even higher strain values, arm-chair and zig-zag chains undergo a transition to carbene chains. As in the case of graphene, and for similar reasons, the experimental procedure of fracture is expected to be complicated with diverse products and differences in break points.

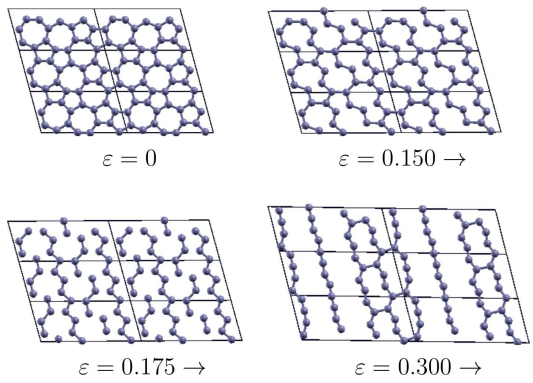

FIG. 8: Snapshots of PeHe-B for strains along e_{a2}. The arrows show the strain direction.

C. Strain as a synthetic route factor

As already shown, at equilibrium PeHe-A, PeHe-B and OcGr are energetically higher than graphene and a 90° rotation of a bond has an energy cost of the order of 1.8-2.0 eV. However, this energy cost might be eliminated upon tensile strain of graphene in certain directions, which in turn would favour the conversion of graphene to its allotropes. In the present work we atempt to find possible strain pathways which favour the SWTs presented in Fig. 1, leading to the conversion of graphene to PeHe-A, PeHe-B and OcGr.

For this conversion scenario, we consider graphene strained along a certain direction. Then, SWTs are carried out in the strained graphene structure, if they are favoured by strain in that direction. In principle, the resulting allotrope structure would be also strained along the same strain direction and hopefully, upon strain release, it leads to its equilibrium structure. For the conversion of graphene to PeHe-A and PeHe-B, those SWTs are shown with the red colored bonds in the top and bot-

tom panels of Fig. 1, respectively, while for its conversion to OcGr there are two different set of SWTs, corresponding to the rotation of the red and orange coloured bonds in the top (pathway A) and bottom panel (pathway B) of Fig. 1.

This conversion proccess requires the existance of a crossing point in the plots of the total energy versus strain of graphene and its allotrope both strained along the same strain direction. Such crossing points for differenet strain directions, do not constitute possible conversion pathways, and therefore they are not of interest. Moreover, if such a crossing point exists, then, in order for a transition from graphene to an allotrope to occur, (i) the strain corresponding to the crossing point must be considerably less than fracture strain and (ii) the energy barrier for the necessary SWTs must be small.

The existence of crossing points for any direction (n, m) (in fractional coordinates with respect to the rectangular unit cell vectors) can be tested qualitatively, with a harmonic approximation for the total energy U of graphene and its allotropes. If such crossing points appear in the regions of large strains, (i.e. in the non elastic regime, where the harmonic approximation can not apply), this procedure serves as a qualitative analysis for those points, to identify the directions that such points exist.

Writing $U = k\varepsilon^2 + U_0$, where $k = Ev/2$, E is the Young's modulus and v the atomic volume, and equating the cohesive energies of graphene and the allotrope at a strained lattice parameter a along a specific direction (n, m), we obtain

$$k_g(a - a_g)^2/a_g^2 = k_a(a - a_a)^2/a_a^2 + \Delta U. \qquad (3)$$

The indices g and a refer to graphene and the allotrope, respectively, and ΔU is their total energy difference at their equilibrium distances. a_g and a_a are corresponding equilibrium lattice parameters along the direction (n, m), i.e. $a_g = (n^2 a_{g,x}^2 + m^2 a_{g,y})^{1/2}$ and $a_a = (n^2 a_{a,x}^2 + m^2 a_{a,y}^2)^{1/2}$, where $a_{g,x}$, $a_{g,y}$ and $a_{a,x}$, $a_{a,y}$ are the lattice parameters along x and y directions for graphene and its allotrope, respectively. A similar relation could be written for the conversion of an allotrope to another one, like for instance the conversion of PeHe-A or PeHe-B to OcGr, according to the SWTs corresponding to the rotation of the orange colored bonds in the top and bottom panels of Fig. 1(e), respectively. It is worth notting that the reversal of the order of the SWTs corresponding to the rotation of the orange and red colored bonds of Fig. 1, does not consitute any extra conversion pathway, since the SWTs of either the red or the orange colored bonds in graphene lead to the same allotrope structure.

For the investigation of the conversion of graphene to PeHe-A and PeHe-B, let us assume for simplicity that PeHe-A and PeHe-B are isotropic, i.e. k_a is independent on the strain direction. Using the obtained values for E, we find $k_g \approx 28$ eV for graphene, $k_a \approx 24$ eV for PeHe-A, and ≈ 26 eV for PeHe-B. Solving Eq. 3 with respect to a and imposing that $a < 1.3a_g$, we arrive at the conditions $|m| < 2.94|n|$ (for PeHe-A) and $|m| > 1.33|n|$ (for PeHe-B) for the existence of crossing points along the direction (n, m). Among the high symmetry strain directions considered in this work for graphene, only e_{a1} and e_{z2} for for its convertion to PeHe-A, and e_{z1} and e_{a2} for its convertion to PeHe-B satisfy these conditions.

On the other hand, for the investigation of the conversion of graphene, PeHe-A and PeHe-B to OcGr, k_a depends not only on the strain direction, but also on the SWTs, which take place for such a convertion. More details on the estimation of k_a for patheway A and B for different strain directions are presented in the Supplemental Information.

Following the above methodology for those estimated k_a values, we find the strain directions that favour the formation of OcGr. According to our findings, strain favours the conversion to OcGr (i) of PeHe-A, for all strain directions, (ii) of graphene under the SWTs of pathway A, for all strain directions, (iii) of graphene under the SWTs of pathway B, for the strain directions with $|m| > 0.920|n|$, (iv) of PeHe-B, for the strain directions with $|m| > 0.644|n|$. Consequently, among the structures and the considered strain directions of our study, only graphene under the SWTs of pathway B and PeHe-B, both strained along e_{a1} direction, do not favour the formation of OcGr.

The results of the above qualitative analysis, are confirmed by our DFT calculations. This is clearly shown in Fig. 9.

Fig. 9(a) shows the total energy of graphene obtained from our DFT calculations, as a function of its lattice parameter for strain along e_a directions (i.e. e_{a1}, e_{a2} and e_{a3} directions), which (as mentioned) are equivalent for graphene. In the same graph we show the DFT results for the total energy of PeHe-A strained along e_{a1} and PeHe-B strained along e_{a2} direction, the formation of which is favoured (according to the above qualitative analysis) from strained graphene along these directions under the corresponding SWTs of Fig. 1. We also shown the total energy of OcGr strained along e_{se} direction, the formation of which is predicted from the above qualitative analysis, from strained graphene along e_{a1} direction, under the SWTs of pathway A. As one can see, graphene strained along e_a direction is energetically more favorable than PeHe-A strained along e_{a1} and PeHe-B along e_{a2} direction until 1.10 $a_{g,x}$, i.e. for $\varepsilon < 10\%$, while for higher strains, the periodic net of SWTs leading to either PeHe-A or PeHe-B leads to energy lowering. Apart from a tiny region beyond the crossing point, that PeHe-A is energetically lower, PeHe-B appears to be the optimal for a broad region of the lattice parameter. OcGr strained along e_{se} direction becomes energetically more favorable than graphene and PeHe-A both strained along e_{a1} direction, for $a > 1.15\, a_{g,x}$ and $a > 1.22\, a_{g,x}$, respectively, corresponding to 15 % strain for graphene and 14 % for PeHe-A.

Similarly, Fig. 9(b) shows the total energy of graphene

obtained from our DFT calculations, as a function of its lattice parameter for strain along the three equivalent e_z directions, together with the total energy of PeHe-A strained along e_{z2} and PeHe-B strained along e_{z1}, the formation of which is favoured (according to the above qualitative analysis) from strained graphene along these directions. We also show the total energy of OcGr strained along both e_{se} and e_{sd} directions, since their formation from strained graphene along e_{a1} direction, has been predicted to be favoured from the above qualitative analysis, under the SWTs of pathway A and B, respectively. As one can see, graphene strained along e_z direction is energetically less favorable than PeHe-A strained along e_{z2}, PeHe-B along e_{z1} and OcGr along e_{sd} direction, for $a > 1.12\,a_{g,y}$, $1.13\,a_{g,y}$ and $1.23\,a_{g,y}$, respectively, (i.e. for $\varepsilon > 12$ %, 13 % and 23 %, respectively). Those strain values are larger than the corresponding values for the arm-chair directions for those structures. Moreover, PeHe-B strained along e_{z1} direction is less favorable than OcGr along e_{sd} for $a > 1.33\,a_{g,y}$, corresponding to strain $\varepsilon = 12$ % for PeHe-B. As seen, the energeticaly more favourable structure for $1.12\,a_{g,y} < a < 1.33\,a_{g,y}$ is PeHe-B strained along e_{z1} direction, while for $a < 1.33\,a_{g,y}$, is OcGr strained along e_{sd}.

In contrast to the above qualitative analysis, Fig. 9(b) shows that there is not any crossing point of the energy curves of graphene strained along e_{z1} and OcGr strained along e_{se} directions. According to the harmonic approximation prediction, that crossing point should appear at graphene strain value $\varepsilon \approx 21$ %. However, for that high strain value of graphene, the harmonic approximation is not so accurate, due to the softening of graphene, as shown in Fig. 2(a), resulting to a bending of the total energy curve towards larger strain values, thus avoiding the crossing with the OcGr energy curve. Consequently, this discrepancy is attributed to the anharmonicity of graphene for such large strains. Thus, in contrast to the results of our qualitative analysis, the conversion of strained graphene to OcGr through pathway A is not favoured for strain directions close to e_{z1}.

In Fig. 9(b) we also show the total energy of PeHe-A strained along e_{z1}, although graphene strained along this direction does not favour its formation. However, PeHe-A strained along e_{z1} favours the formation of OcGr (crossing point of the energy curves of PeHe-A strained along e_{z1} and OcGr strained along e_{se}). This is an example of conversion of strained graphene to an intermediate structure (PeHe-A) and then conversion of that structure to OcGr favoured by different strain directions.

The obtained strain values for the crossing points are extreme, however, they are substantially lower than the experimentally measured value $\varepsilon_u = 0.25$, corresponding to the UTS for graphene[42]. The directions that crossing points are found are those that the rotating bonds turn into or minimize their angle with, when the corresponding SWTs take place which result to an elongation of lattice parameter in those directions, as a stress reduction mechanism. Indeed, given that the Young's moduli

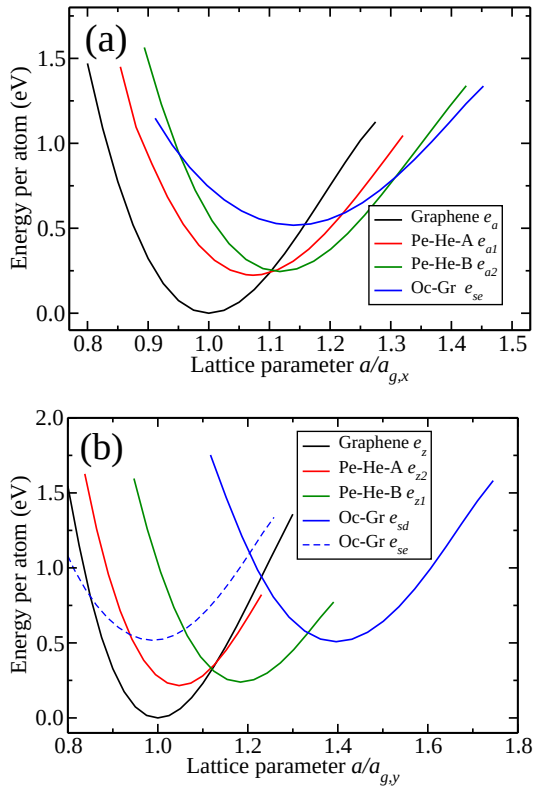

FIG. 9: Total energy per atom versus lattice parameters for the zig-zag and armchair directions, respectively.

of graphene and the pentaheptites do not differ dramatically, the existence of crossing points is mostly the result of the enlargement of the equilibrium lattice parameters for the allotropes compared with graphene in those directions.

Even if they lead to energetically favored structures, SWTs can only take place if the energy barriers separating the structures are overcome. At ambient strain that barrier (7-9 eV) is rather prohibitive[6,36]. In order to estimate the dependence of the energy barrier of SWTs on the strain, we performed transition-state calculations on a strained pyrene molecule, shown in Fig. 10(top)(a), using Gaussian 09 program[54] with B3LYP functional[55,56] and the 6-31G* basis set. The strain was applied by freezing the distances between atoms 3,4 and 5,6 (Fig. 10 top panel, (a)) while the geometry of the transition state (b) was optimized. In Fig. 10(bottom), we see that the energy difference ΔE of the structure with SWT is reduced with strain and become energetically favorable for a strain $\sim 12\%$ in consistency with our periodic DFT calculations. In addition, the energy barrier, E_b, for the SWT is reduced substantially from ~ 8.5 eV to less than 5 eV for large strains in agreement with atomistic simulations[39]. Despite its substantial reduction this barrier remains large enough and prohibitive for SWTs. However, due to this substantial reduction, strain may become a possible assisting factor for the synthesis of these allotropes in the future.

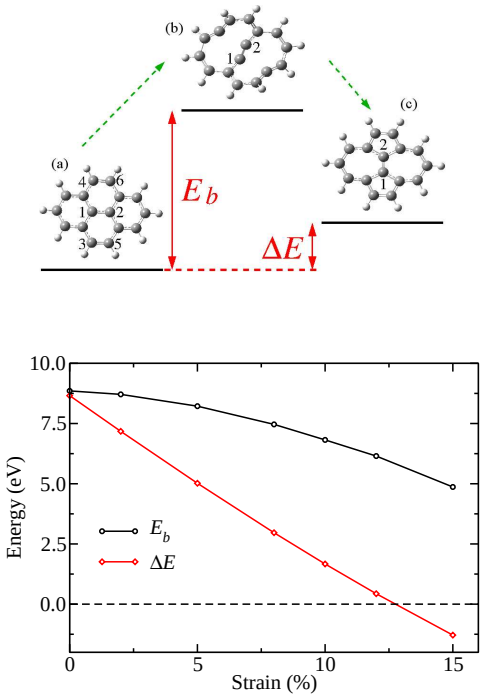

FIG. 10: The transition diagram of pyrene molecule (top), as well as the transition state energy E_b and the energy difference ΔE of (c) from (a) as a function of uniaxial strain (bottom).

IV. CONCLUSIONS

Performing ab-initio DFT calculations, we study the response of representative periodic graphene allotropes (namely two pentaheptites and octagraphene) to uniaxial strain for several high symmetry strain directions in comparison with graphene. Those graphene allotropes can be derived from graphene upon extensive, periodically arranged SWTs. Based on this, we study strain as a possible assisting factor for SWTs, which could make possible the synthesis of these structures from graphene.

According to our findings, pentaheptites are quite isotropic in terms of strength and Poisson's ratio, while octagraphene is not. The allotropes of our study exhibit high Young's modulus, speed of sound and UTS values, which are comparable to graphene, although smaller. Poisson's ratio is higher in pentaheptites than in graphene. For octagraphene strained along the square-diagonal direction it is similar to graphene, and for the square-edge direction it is much higher. For strain values higher than the corresponding to the UTS, the structures of our study either dissociate to linear chains, or they undergo phase transition to structures containing carbene units.

For strains exceeding in value 12% and 10% for zigzag and arm-chair directions, respectively, graphene become less favorable energetically than its pentaheptite allotropes. Although extreme, these values of strain are still smaller than the experimentally identified strain of 25% corresponding to the UTS of graphene. The energy barrier upon strain for the transition to these allotropes remains quite prohibitive, however, it is reduced significantly from 7-9 eV to 4-5 eV, allowing the possibility that strain could become an assisting factor for their synthesis from graphene, in combination with other processes like for instance catalysis or irradiation.

Acknowledgments

NNL acknowledges support from the Thales Project GRAPHENECOMP, financed by the EU (ESF) and the Hellenic Ministry of Education (through ΕΣΠΑ) and from the GSRT action ΚΡΗΠΙΣ, project "New multifunctional Nanostructured Materials and Devices - POLYNANO". ZGF acknowledges financial support from the National Science Foundation Cooperative Agreement No. EEC-0832785, titled "NSEC: Center for High-rate Nanomanufacturing".

[1] K. S. Novoselov, D. Jiang, F. Schedin, T. J. Booth, V. V. Khotkevich, S. V. Morozov, and A. K. Geim, Proc. Nat. Acad. Sci. **102**, 10451 (2005).
[2] D. Pacilé, J. C. Meyer, C. O. Girit, and A. Zettle, Appl. Phys. Lett. **92**, 133107 (2008).
[3] Y. Lin and J. W. Connell, Nanoscale **4**, 6908 (2012).
[4] Q. H. Wang, K. Kalantar-Zadeh, A. Kis, J. N. Coleman, and M. S. Strano, Nature Nanotech. **7**, 699 (2012).
[5] A. N. Enyashin and A. L. Ivanovskii, Phys. Stat. (b) **248**, 1879 (2011).
[6] V. H. Crespi, L. X. Benedict, M. L. Cohen, and S. G. Louie, Phys. Rev. B **53**, R13303 (1996).
[7] M. T. Lusk and L. D. Carr, Phys. Rev. Lett. **100**, 175503 (2008).
[8] M. T. Lusk, D. T. Wu, and L. D. Carr, Phys. Rev. B **81**, 155444 (2010).
[9] X.-Q. Wang, H.-D. Li, and J.-T. Wang, Phys. Chem. Chem. Phys. **15**, 2024 (2013).
[10] H. Terrones, M. Terrones, E. Hernández, N. Grobert, J.-C. Charlier, and P. M. Ajayan, Phys. Rev. Lett. **84**, 1716 (2000).
[11] S. J. Stone and D. J. Wales, Chem. Phys. Lett. **128**, 501 (1986).
[12] P. A. Thrower, *The study of defects in graphite by transmission electron microscopy*, vol. 5 of *Chemistry and Physics of Carbon* (Marcel Dekker, New York, 1969).
[13] X. Rocquefelte, G.-M. Rignanese, V. Meunier, H. Terrones, M. Terrones, and J.-C. Charlier, Nano Letters **4**, 805 (2004).
[14] X.-L. Sheng, H.-J. Cui, F. Ye, Q.-B. Yan, Q.-R. Zheng, and G. Su, J. Appl. Phys. **112**, 074315 (2012).
[15] Y. Liu, G. Wang, Q. Huang, L. Guo, and X. Chen, Phys.

Rev. Lett. **108**, 225505 (2012).
[16] H. Q. Huang, Y. C. Li, Z. R. Liu, J. Wu, and W. H. Duan, Phys. Rev. Lett. **109**, 269601 (2012).
[17] H. Huang, Y. Li, Z. Liu, J. Wu, and W. Duan, Phys. Rev. Lett. **110**, 029603 (2013).
[18] Y. Liu, G. Wang, Q. Huang, L. Guo, and X. Chen, Phys. Rev. Lett. **110**, 029602 (2013).
[19] Y. Liu, G. Wang, Q. Huang, L. Guo, and X. Chen, Phys. Rev. Lett. **110**, 269604 (2013).
[20] G. Mpourmpakis, G. E. Froudakis, and E. Tylianakis, Appl. Phys. Lett. **89**, 233125 (2006).
[21] S. Lisenkov, A. N. Andriotis, I. Ponomareva, and M. Menon, Phys. Rev. B **72**, 113401 (2005).
[22] Z. G. Fthenakis, Z. Zhu, and D. Tománek, Phys. Rev. B **89**, 125421 (2014).
[23] C. Su, H. Jiang, and J. Feng, Phys. Rev. B **87**, 075453 (2013).
[24] X.-Q. Wang, H.-D. Li, and J.-T. Wang, Phys. Chem. Chem. Phys. **14**, 11107 (2012).
[25] M. T. Lusk and L. Carr, Carbon **47**, 2226 (2009).
[26] G. Brunetto, P. A. S. Autreto, L. D. Machado, B. I. Santos, R. P. B. dos Santos, and D. S. Galvo, J. Phys. Chem. C **116**, 12810 (2012).
[27] J. Kotakoski, A. V. Krasheninnikov, U. Kaiser, and J. C. Meyer, Phys. Rev. Lett. **106**, 105505 (2011).
[28] J. C. Meyer, C. Kisielowski, R. Erni, M. D. Rossell, M. F. Crommie, and A. Zettl, Nano Lett. **8**, 3582 (2008).
[29] F. R. Eder, J. Kotakoski, U. Kaiser, and J. C. Meyer, Sci. Rep. **4**, 4060 (2014).
[30] J. Lahiri, Y. Lin, P. Bozkurt, I. I. Oleynik, and M. Batzill, Nat. Nanotechnol. **5**, 326 (2010).
[31] P. Y. Huang, C. S. Ruiz-Vargas, A. M. van der Zande, W. S. Whitney, M. P. Levendorf, J. W. Kevek, S. Garg, J. S. Alden, C. J. Hustedt, Y. Zhu, et al., Nature **469**, 389 (2011).
[32] P. Simonis, C. Goffaux, P. Thiry, L. Biro, P. Lambin, and V. Meunier, Surf. Sci. **511**, 319 (2002).
[33] E. Cockayne, G. M. Rutter, N. P. Guisinger, J. N. Crain, P. N. First, and J. A. Stroscio, Phys. Rev. B **83**, 195425 (2011).
[34] J. N. B. Rodrigues, P. A. D. Gonçalves, N. F. G. Rodrigues, R. M. Ribeiro, J. M. B. Lopes dos Santos, and N. M. R. Peres, Phys. Rev. B **84**, 155435 (2011).
[35] R. Zan, Q. M. Ramasse, U. Bangert, and K. S. Novoselov, Nano Lett. **12**, 3936 (2012).
[36] L. Li, S. Reich, and J. Robertson, Phys. Rev. B **72**, 184109 (2005).
[37] C. Ewels, M. Heggie, and P. Briddon, Chem. Phys. Lett. **351**, 178 (2002).
[38] M. Kabir, S. Mukherjee, and T. Saha-Dasgupta, Phys. Rev. B **84**, 205404 (2011).
[39] G. G. Samsonidze, G. G. Samsonidze, and B. I. Yakobson, Comp. Mater. Sc. **23**, 62 (2002).
[40] J.-M. Leyssale, G. L. Vignoles, and A. Villesuzanne, J. Chem. Phys. **136**, 124705 (2012).
[41] R. Andrew, R. Mapasha, A. Ukpong, and N. Chetty, Phys. Rev. B **85**, 125428 (2012).
[42] C. Lee, X. Wei, J. W. Kysar, and J. Hone, Science **321**, 385 (2008).
[43] P. Giannozzi, S. Baroni, N. Bonini, M. Calandra, R. Car, C. Cavazzoni, D. Ceresoli, G. L. Chiarotti, M. Cococcioni, I. Dabo, et al., J. Phys.: Cond. Matter **21**, 395502 (19pp) (2009).
[44] J. P. Perdew, K. Burke, and M. Ernzerhof, Phys. Rev. Lett. **77**, 3865 (1996).
[45] A. Dal Corso, URL `http://www.quantum-espresso.org/wp-content/uploads/upf_files/C.pbe-rrkjus.UPF`.
[46] A. M. Rappe, K. Rabe, E. Kaxiras, and J. Joannopoulos, Phys. Rev. B **41**, R1227 (1990).
[47] F. Liu, P. Ming, and J. Li, Phys. Rev. B **76**, 064120 (2007).
[48] X. Wei, B. Fragneaud, C. Marianetti, and J. Kysar, Phys. Rev. B **80**, 205407 (2009).
[49] G. Kalosakas, N. N. Lathiotakis, C. Galiotis, and K. Papagelis, J. App. Phys. **113**, 134307 (2013).
[50] O. Frank, G. Tsoukleri, J. Parthenios, K. Papagelis, I. Riaz, R. Jalil, K. S. Novoselov, and C. Galiotis, ACS nano **4**, 3131 (2010).
[51] E. Cadelano, P. Palla, S. Giordano, and L. Colombo, Phys. Rev. Lett. **102**, 235502 (2009).
[52] Q. Lu and R. Huang, Int. J. Appl. Mech. **01**, 443 (2009).
[53] Z. G. Fthenakis and N. N. Lathiotakis, *Anisotropic mechanical properties of octagraphene*, to be published.
[54] M. J. Frisch, G. W. Trucks, H. B. Schlegel, G. E. Scuseria, M. A. Robb, J. R. Cheeseman, G. Scalmani, V. Barone, B. Mennucci, G. A. Petersson, et al., *Gaussian09 Revision D.01*, gaussian Inc. Wallingford CT 2009.
[55] A. Becke, J. Chem. Phys. **98**, 5648 (1993).
[56] P. Stephens, F. Devlin, C. Chabalowski, and M. Frisch, J.Phys.Chem. **98**, 11623 (1994).
[57] J. Ma, D. Alfè, A. Michaelides, and E. Wang, Phes. Rev. B **80**, 033407 (2009).
[58] A SWT is the rotation of a bond around its center by 90°, which results in the conversion of a pyrene unit (composed of four hexagons, which are adjacent to the rotated bond), to two pentagons and two heptagons.
[59] An isolated SW defect results in local buckling of graphene[7,57].